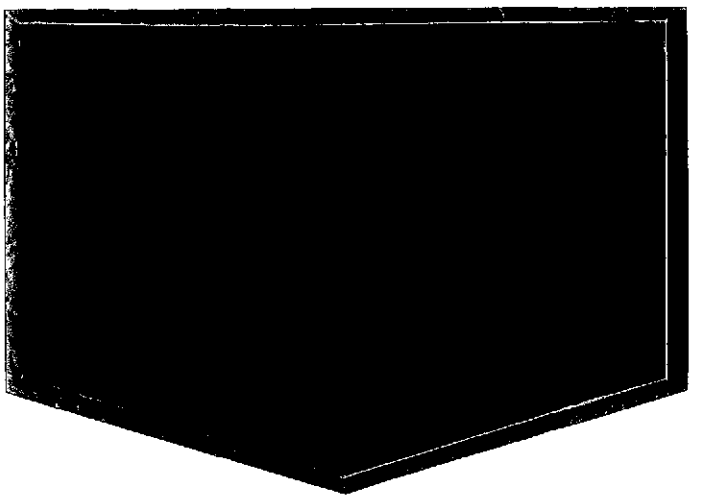

BALL BROTHERS

RESEARCH CORPORATION

BALL BROTHERS RESEARCH CORPORATION

BOULDER, COLORADO

F73-08

Final Report

SEC Vidicon Testing

UCAR Contract No. NCAR 23-73

September 28, 1973

The work under this Subcontract was funded by UCAR's Prime Contract NSF-C760 with the National Science Foundation through a transfer of funds from the National Aeronautics and Space Administration.

PREPARED

D. S. Johnson, Jr.

A. A. Olsen

Senior Members Technical Staff

APPROVED

E. L. Vande Noord

E. L. Vande Noord

Study Leader

NASA Order No. W-13398

FOREWORD

This Final Report is submitted in accordance with the requirements set forth in UCAR Contract No. 23-73 and satisfies the requirements specified in Items 1 and 3 of the statement of work.

BBRC gratefully acknowledges the technical assistance provided by discussions with John L. Lowrance and Paul M. Zucchino of Princeton University relative to the construction of the slow scan test console and pre-amplifier.

SUMMARY

This report presents results obtained from several basic measurements of the performance of an SEC vidicon camera head. The measurements or tests are patterned around the sensor requirements which exist for a Rapid Response Coronagraph. The vidicon used for these tests is a meshless Westinghouse WX 31958, Class III tube. Following a brief description of the SEC vidicon camera head, test set-up, and operating procedures, results are presented for five basic tests. These tests include: 1) input-output, or transfer, characteristics, 2) modulation transfer function, 3) signal-to-noise ratio, 4) photocathode sensitivity, and 5) target gain. The input-output characteristics and photocathode sensitivity measurements were obtained for three bandpasses centered about 4000, 5250, and 6200 Å. Results are also given for the variation of photocathode sensitivity with position on the cathode surface.

It is concluded that the meshless SEC will satisfy the sensor requirements for the RRC, but the camera head electronic system requires additional improvements.

CONTENTS

ILLUSTRATIONS

ILLUSTRATIONS continued

TABLES

Section 1
INTRODUCTION

The present study and measurement program is part of a continuing effort directed towards the development of a Rapid Response Coronagraph (RRC) for the High Altitude Observatory. The RRC will be used to obtain detailed spatial and high temporal resolution measurements of the solar corona from unmanned space platforms. In order to operate without the direct assistance of man, an electronc imaging system will replace the film cameras which were used on the Skylab White Light Coronagraph.

During a previous study[1] which resulted in the preliminary design of an RRC for the OSO-K mission, a meshless secondary electron conduction (SEC) vidicon was selected as the optimum detector. The OSO-K study also led to the conclusion that additional study and testing of the SEC vidicon was required in order to obtain improved design information, to identify problem areas, and to develop performance specifications, procurement guidelines, and test procedures.

This report presents the results of several basic tests or measurements of the SEC vidicon performance which are patterned around the RRC requirements. These RRC performance requirements are summarized in Table 1-1. The five basic tests are as follows:

- Input-Output, or Transfer Characteristics (in absolute radiometric units)
- Modulation Transfer Function (MTF)

---

[1] Preliminary Feasibility Study of a Rapid Response Coronagraph for Operation on the OSO-K Satellite, BBRC Final Report, UCAR Contract NCAR 11-72, 1972.

- Signal-to-Noise Ratio (S/N)
- Photocathode Sensitivity (Integrated and in three spectral bandpasses)
- Target Gain

The first three of these tests involve the overall performance of the vidicon camera head whereas the latter two tests deal with specific subassemblies.

In the following sections, the SEC Vidicon camera head, test console, and auxiliary test apparatus are briefly described, the results of the various tests and measurements are presented, and finally, the study conclusions are summarized.

Table 1-1
PERFORMANCE REQUIREMENTS FOR RRC

Spatial		
•	Extent	1.5 to 6 $R_\odot$
•	Resolution	7.5 arc seconds (System MTF = 27%)
•	Format	Sector FOV (60° wedges)
•	Pointing Accuracy	20 arc seconds
* •	Offset Pointing	Capability of moveable External Occulting Disc Assembly (EODA)
Spectral		
•	Range	4000 to 7000 Å
* •	Intervals	Single Broadband (4861 to 5876 Å)
		Three Bandpass (Center wavelengths approximately 4000, 5200, 6200 Å; bandpass 300 to 500 Å)
		Line Rejection (< 1% for H_α, H_β, He_I)
Intensity		
•	Accuracy	1 to 2%
Temporal		
•	Time Betwen Pictures	< 20 seconds
Other		
•	Three Polarization Measurements	
•	Calibration Wedge Exposed on Selected Pictures	
•	Single Picture is Average of Two Exposures	

* Requirement developed since conclusion of OSO-K RRC Study Contract.

Section 2
SYSTEM DESCRIPTION

Background

Evaluation of a photoelectronic imaging sensor, such as an SEC vidicon, in general requires measurement of its performance as part of a complete system. The sensor requires externally generated magnetic fields for focus and scanning functions and it must have a programmed sequence of voltages and currents applied to it which is tailored to achieve optimum performance for a particular application. The low-level sensor output signal must be amplified and band-limited in a manner that maximizes the signal-to-noise ratio. The quality of the system output signal, therefore, is not only a function of the camera tube itself, but is also dependent on the quality of the magnetic focus and deflection fields, the noise level of the amplifier, the accuracy and stability of the applied potentials, and the proper programming of the entire system for the specific application at hand.

2.1 TEST SET-UP

The test set-up is comprised of two basic units. The first is the camera head which contains the SEC vidicon tube, the focus, deflection, and alignment coils, and the low noise pre-amplifier. The second unit is the slow scan test console which houses the master control clock, digital sweep generators, voltage programming circuits, and several power supplies.[2] The relationship of

---

[2] The SEC Vidicon and deflection coils were supplied by HAO; the focus coil and pre-amplifier were constructed by BBRC as part of the present contract. The slow scan test console was designed and fabricated by BBRC with internal funds. Additional details on the test console are contained in BBRC Technical Note TN 73-09, March 23, 1973.

these units is shown in the simplified block diagram of Figure 2-1, along with the display instrumentation which must receive appropriate timing pulses from the test console.

Figure 2-2 is a symbolic sketch of the camera head showing how the preamplifier and coils are packaged around the SEC vidicon. Not shown is a magnetic shield which encloses the entire assembly, except for a circular opening that provides the entrance for the light beam from the coronagraph optics. This shield not only provides electromagnetic shielding but also helps to shape the focus field in the vicinity of the photocathode. The focus coil provides a uniform magnetic field for focus of the electron image in both the image and readout (gun) sections of the vidicon. A photograph of the partially disassembled camera head, showing the SEC vidicon[3] and the deflection yoke removed from the focus coil, is given in Figure 2-3. Also shown in Figure 2-3 is the shielded, annular preamplifier package which is mounted on the right end of the deflection coil assembly. The entire test set-up, including test console, camera head, X-Y monitor, and auxiliary radiometric equipment, is shown in the photograph of Figure 2-4. Of particular note is the microscope pattern projector, which provides a properly focused optical image of various test targets on the photocathode.

2.2 OPERATION

Camera Head

When an optical image of a 60° sector of the solar corona is focused by the coronagraph optics on the semi-transparent S-20 photocathode, the resultant photoelectrons are accelerated by the 8 KV electric field towards the target. The 80 gauss magnetic field forms an electron image on the low-density KCl target.

---

[3] The particlar tube that was tested is a Westinghouse WX31958, Serial No. 71-47-114, Class III tube.

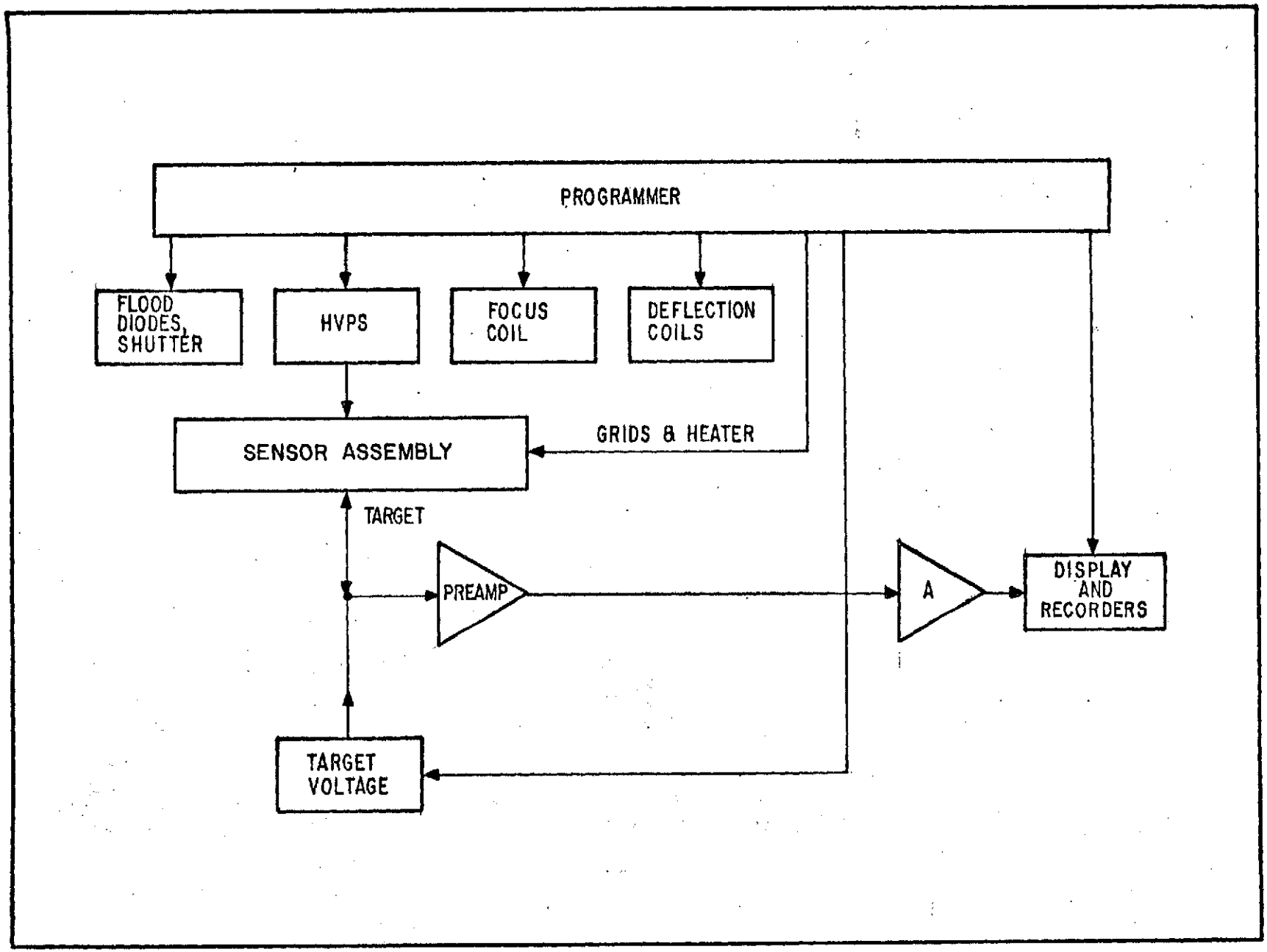

Fig. 2-1 Image Sensor Test Set-Up

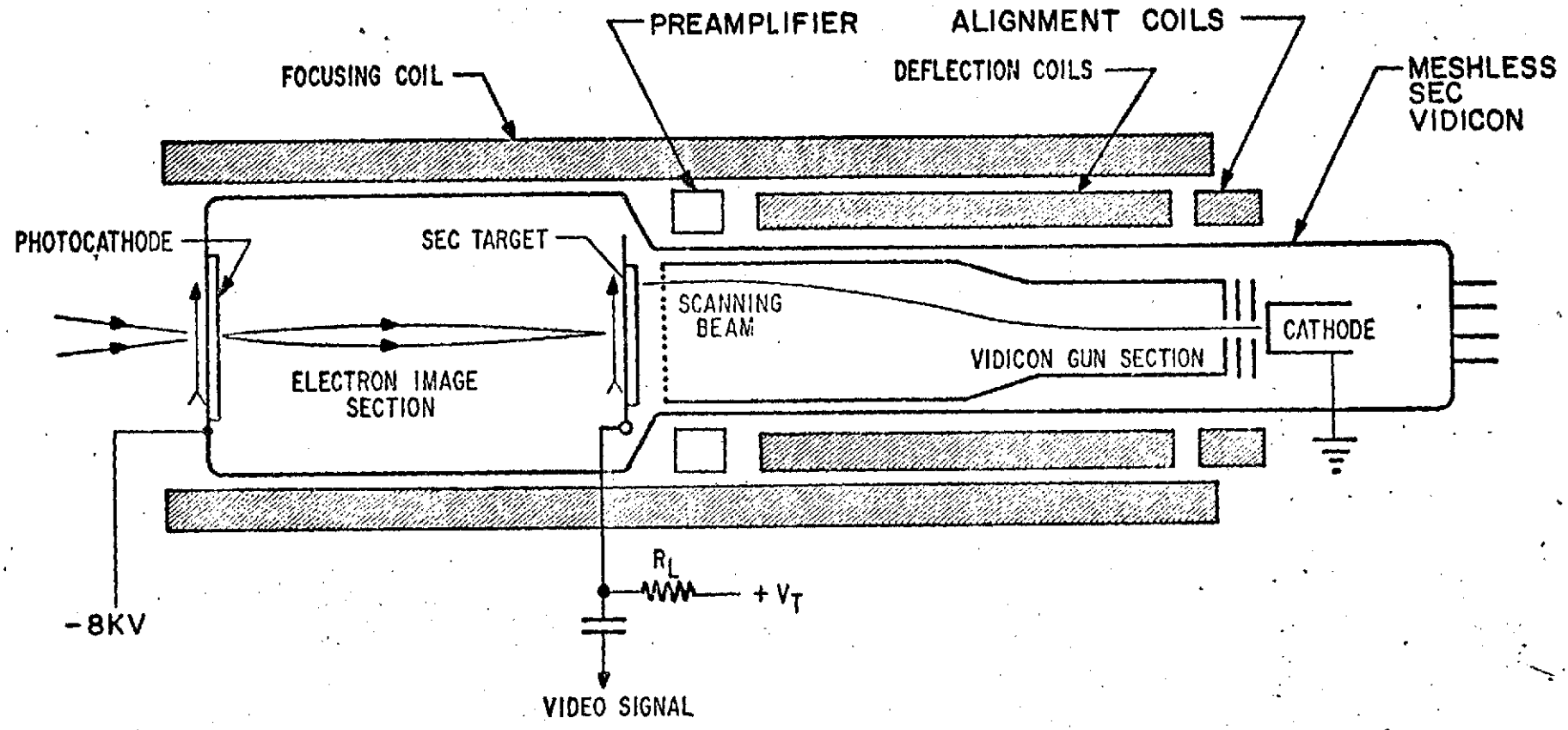

Fig. 2-2 HAO Camera Head (Schematic)

Fig. 2-3 Photograph of HAO Camera Head

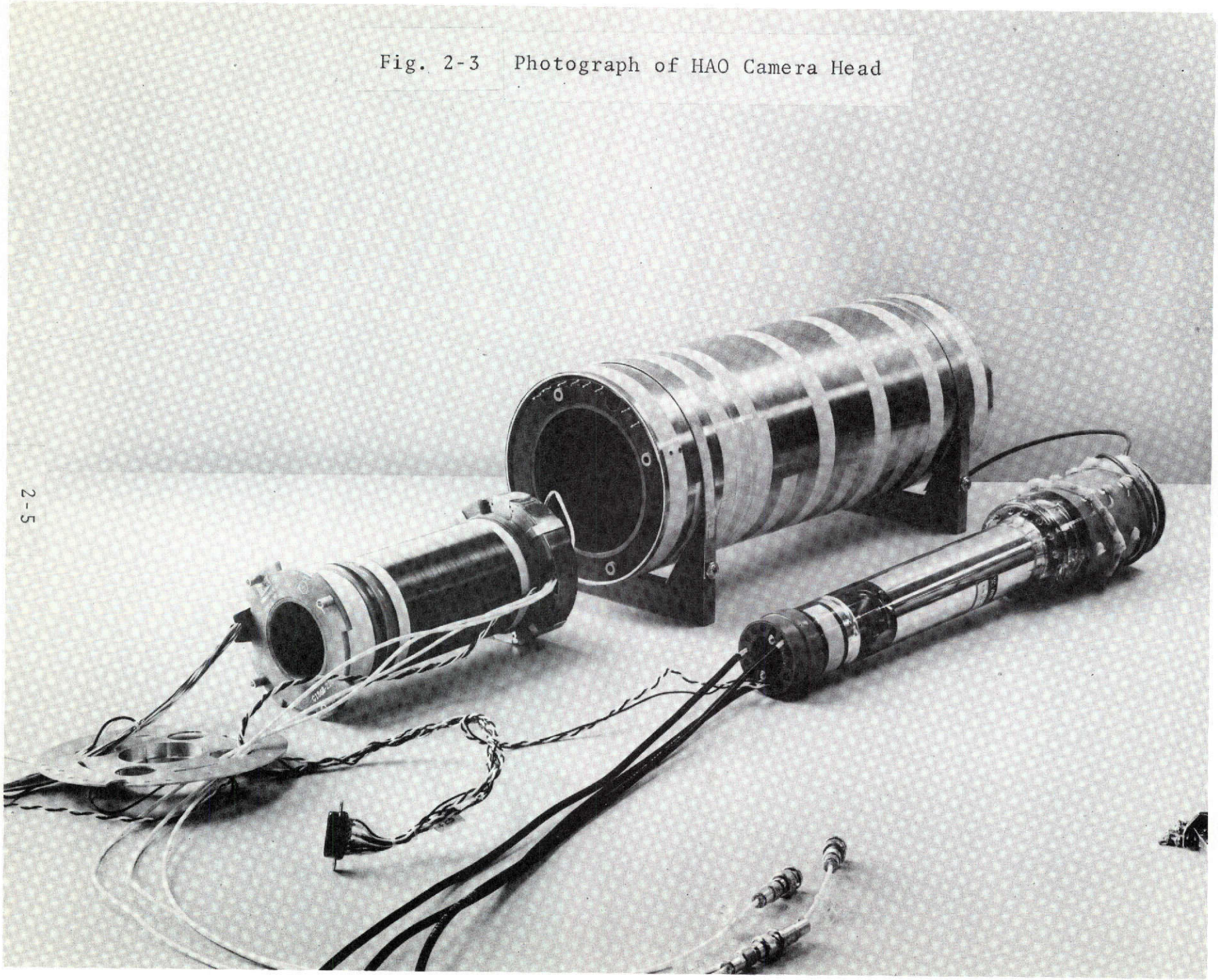

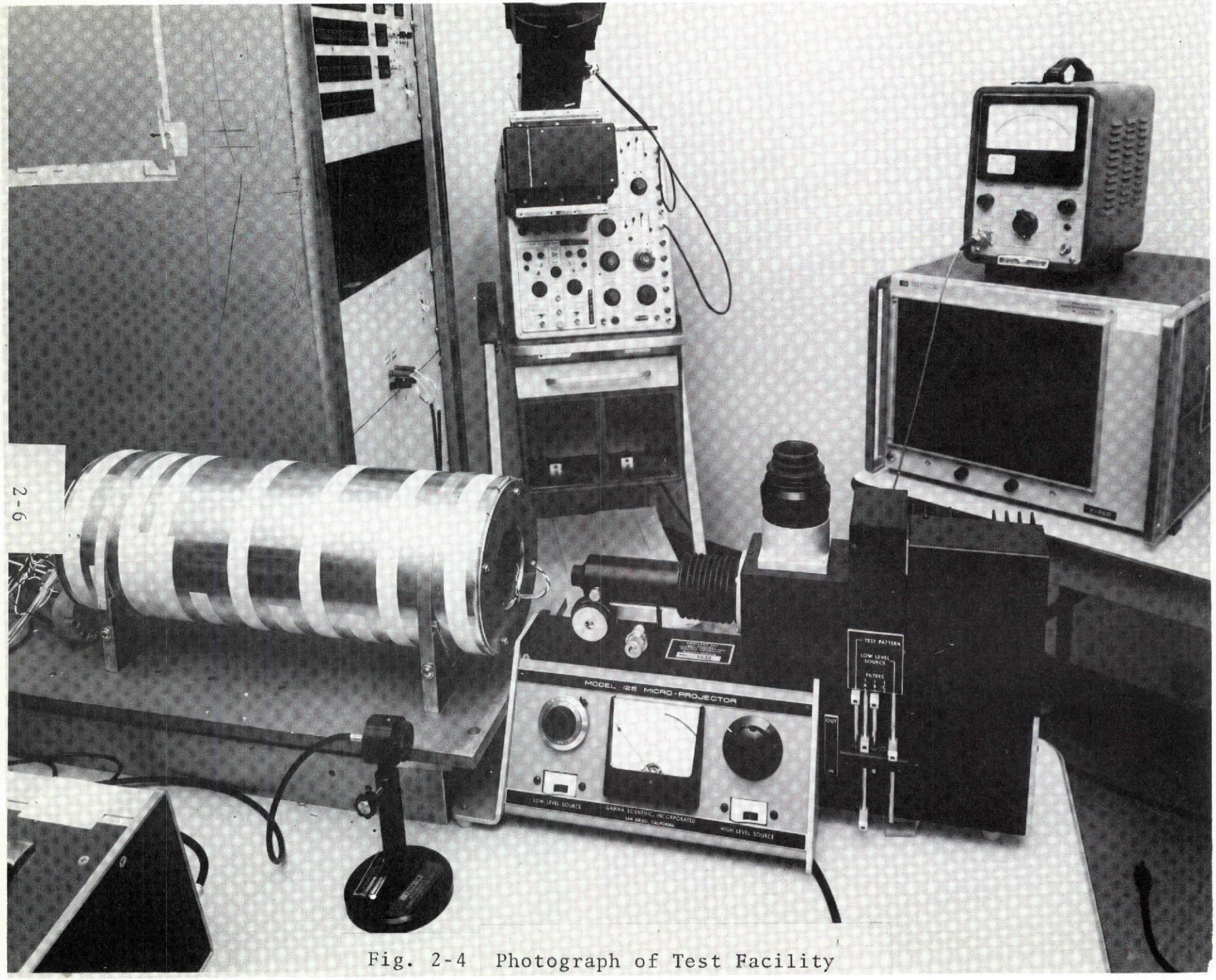

Fig. 2-4 Photograph of Test Facility

Each high-energy primary photoelectron reaching the target creates about 70 secondary electrons. These secondary electrons are free to migrate through the low density target layer in a manner which results in an equal positive charge being built up on the exit surface of the target. During an exposure we have in effect a charge image on the target which builds up as an amplified time integration of the primary electron image. After an exposure, the charge image may be stored for an extended period, if desired, without degradation. The stored pattern is then read-out by scanning the exit side of the target; point-by-point, with an electron beam in the "gun" section of the vidicon. As the target is scanned, the stored charge pattern is sequentially discharged by the beam, generating a time variant output current at the target signal lead. To minimize noise, this low level current is first amplified in a very low-noise current pre-amplifier, which is mounted around the tube neck to keep leads short and shunt capacitance low, before subsequent signal processing.

Slow Scan Test Console

The slow scan test console permits a sequential mode of operation which is specifically tailored to the desired astronomical observing program. In the sequential operating mode, the image sensor is cycled through six modes. They are: ERASE and PREPARE, HOLD, EXPOSE, STORE, RESTORE, and READ. The modes, or cycles, are described as follows:

ERASE AND PREPARE	During this cycle the previous image is erased and the target normalized. The test set provides up to 18 erase frames with the target and grid voltages programmable for each frame. The reason for having such a large number of frames is because certain image sensors such as the SEC vidicon tube require

a certain selection of voltages and sequences to provide optimum erasing.

HOLD — This cycle provides an inactive period prior to the expose and can be used for restoration and preparation of variable parameters in the tube.

EXPOSE — Variable exposure times are provided during this cycle for integrating faint images.

STORE — The store cycle allows storage of the image on the target with the image section off and provides a means of checking the image degradation over a period of time.

RESTORE — The target, grid and focus voltages are allowed to stabilize prior to read out during this cycle.

READ — The target is read out during this cycle. Any combination of grid and target voltages can be programmed in and the scan rate can be adjusted to a slower rate than the erase cycle.

Section 3
MEASUREMENT RESULTS

In the following sub-sections we present results of the five basic tests: photocathode radiant sensitivity, input-output, target gain, modulation transfer function, and signal-to-noise.

3.1 PHOTOCATHODE RADIANT SENSITIVITY

Measurements were made of the photocathode radiant sensitivity integrated over the entire S-20 spectral region as well as bandpass measurements centered about 4000, 5250, and 6200 Å.

This group of measurements of cathode responsivity must be made independently of the characteristics of the other parts of the sensor such as the SEC target, focus fields, electron-beam readout, and so forth. This isolation is achieved by disconnecting all the normal potentials from the tube, allowing the image section to be operated as a simple photodiode. A polarizing potential of about 150 volts is applied between the photoemissive cathode and the effective anode electrode, and a micromicroammeter is put in the loop to measure the photocurrent, as shown in Figure 3-1.

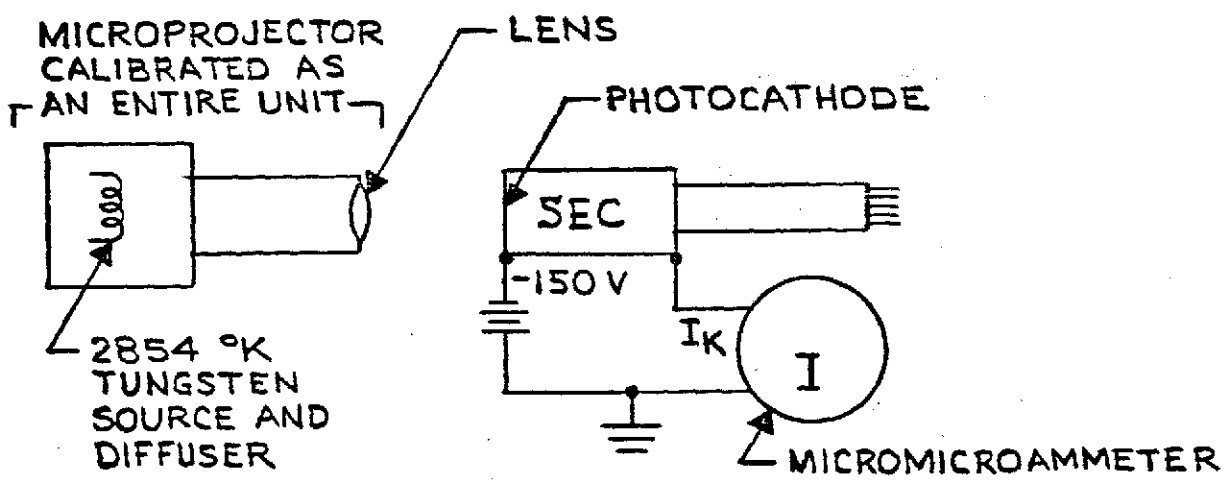

Fig. 3-1 Test Set-up for Measurements of Integrated Photocathode Sensitivity

Integrated Measurements

An approximate determination of the broadband photocathode sensitivity was made by measuring the integrated response to an unfiltered tungsten source operated in the neighborhood of 2854 °K. We used the "high-level" source in the Gamma Scientific microscope projector, normally used for focusing. The projector's lamp, objective lens, and geometry were all calibrated together in terms of image plane illuminance (Lumen/Ft^2), enabling us to measure the photocathode integrated response with tungsten foot-candles in the manner that the tube manufacturers use; that is, in Amp/Lumen. The utility of such a measurement is limited, but it does provide an easy way to verify that the photocathode is indeed functioning properly for an S-20 surface and permits comparison with the similar measurement made by Westinghouse on the same tube.

The results are summarized as follows:

BBRC Measurement:	144 $\pm$ 3 μ amp/lumen
Westinghouse Measurement:	154 μ amp/lumen

Spectral Bandpass Measurements

The radiant sensitivity of the photocathode was also measured for three bandpasses centered about 4000, 5250, and 6200 Å ($\Delta\lambda \sim$ 200-300 Å). A recently calibrated spectral irradiance standard[4] was used with three different bandpass filters to irradiate the photocathode as shown in Figure 3-2. At the vidicon, all electrodes were connected as previously described.

---

[4] Gamma Scientific Lamp Model 220-6, Serial No. 644. Calibrated August 15, 1973.

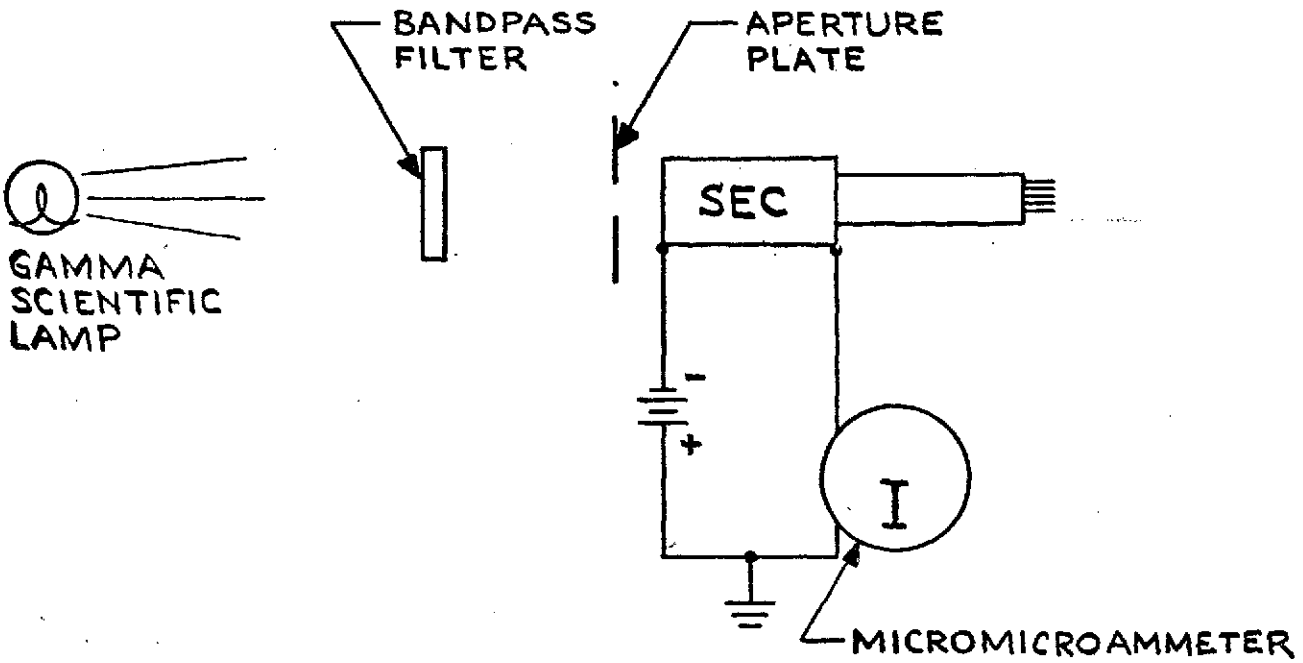

Fig. 3-2 Test Set-up for Bandpass Measurements of Photocathode Sensitivity

In developing the analysis to interpret the test results we use the following notation:

$H_1(\lambda)$	Spectral irradiance at reference distance x_0 $(\frac{\text{watts}}{\text{cm}^2\text{nm}})$
$T(\lambda)$	Spectral Transmittance of filter
$R_0(\lambda)$	Standard S-20 spectral response $(\frac{\text{amp}}{\text{watt}})$
$R(\lambda)$	Actual photocathode response $(\frac{\text{amp}}{\text{watt}})$
$k(\lambda)$	$R(\lambda)/R_0(\lambda)$ (Assumed constant for each filter bandpass)
λ_0	Effective wavelength of flux (Å)
A	Aperture area (cm^2)
S	Cathode current (Amp)

We bring in the "standard" S-20 response, $R_0(\lambda)$, to increase the accuracy of a subsequent integration over wavelength.

The cathode current is a function of a geometric term and the integral over wavelength of several terms:

$$S = \left(\frac{x_0}{x}\right)^2 A \int H_1(\lambda)T(\lambda)R(\lambda)d\lambda \qquad (1)$$

$$= \left(\frac{x_0}{x}\right)^2 Ak \int H_1(\lambda)T(\lambda)R_0(\lambda)d\lambda \qquad (2)$$

After solving this expression for k for each filter used, we then determine the cathode response:

$$R(\lambda_0) = k(\lambda_0)R_0(\lambda_0) \qquad (3)$$

In order to do this, we need the value of the integral in Equation (2) and the value of λ_0 for each filter.

The integrals were solved numerically by computer. The $H_1(\lambda)$ data were taken from calibration data for a lamp at a color temperature of 3200 °K. (The actual tube calibration was done with a lamp at a color temperature of about 2850 °K. The difference in absolute level was ratioed out. The difference in shape of the two curves will cause a neglibible error in the calculation of the effective wavelength.) The filter transmissions $T(\lambda)$ were taken from measurements performed on a Cary 14 spectrophotometer and are shown in Figure 3-3. The standard S-20 response was taken from data supplied by IT&T.

The "effective" wavelength, λ_0, for each combination of source flux, filter, and cathode response, is the wavelength at which the same amount of monochromatic input flux would cause the same output from the photocathode. Neglecting geometry, the input flux to the cathode with a particular filter is

Figure 3-3.

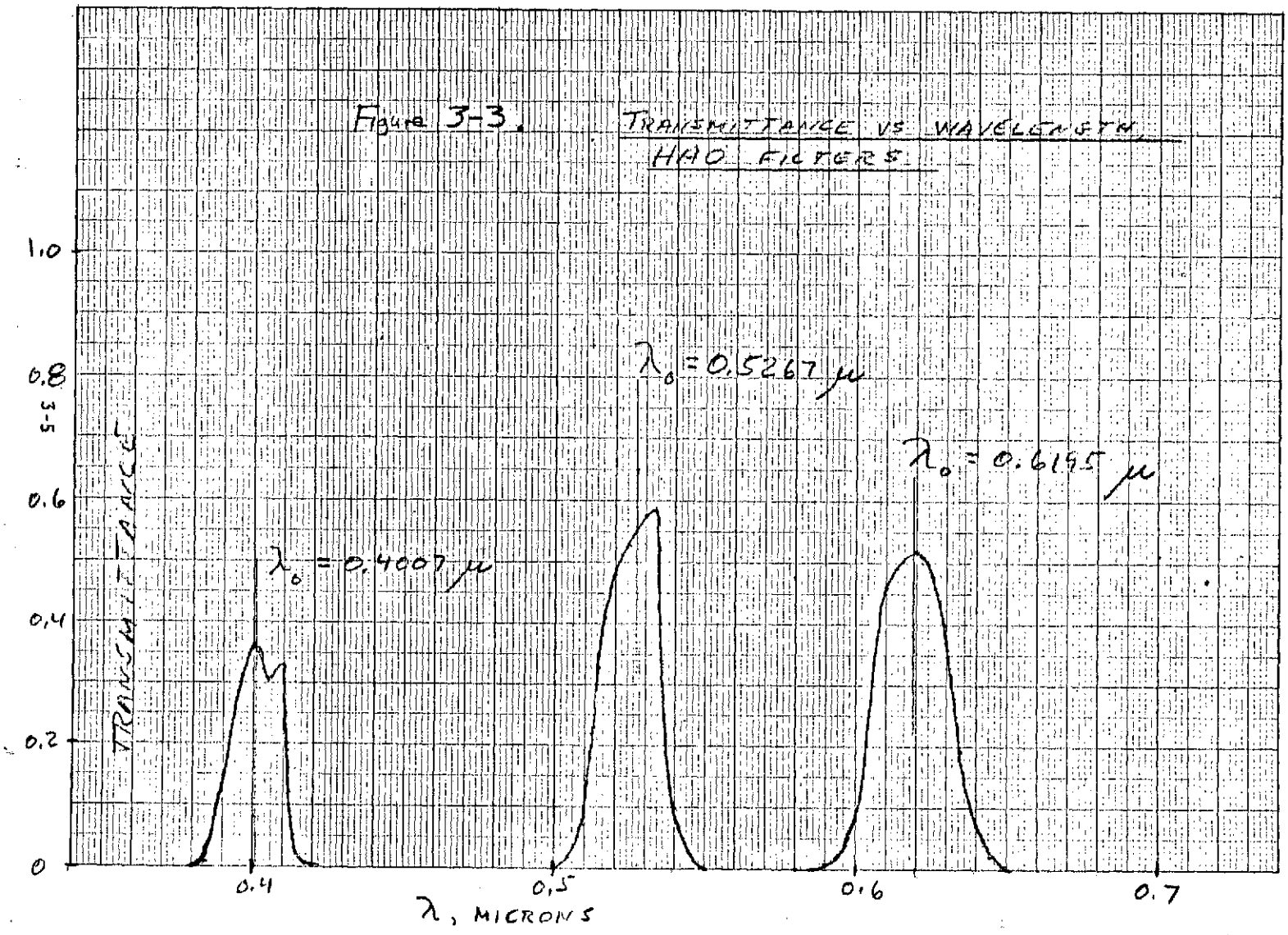

$$H \propto \int T(\lambda)H_1(\lambda)d\lambda \ . \tag{4}$$

The output current of the photocathode is

$$S = \int T(\lambda)H_1(\lambda)R(\lambda)d\lambda \tag{5}$$

$$\cong k\int T(\lambda)H_1(\lambda)R_0(\lambda)d\lambda \ . \tag{6}$$

The output produced with monochromatic flux would be

$$S = HkR_0(\lambda_0) = k\int T(\lambda)H_1(\lambda)R_0(\lambda)d\lambda \ . \tag{7}$$

To find λ_0, we calculate

$$R_0(\lambda_0) = \frac{\int T(\lambda)H_1(\lambda)R_0(\lambda)d\lambda}{\int T(\lambda)H_1(\lambda)d\lambda} \tag{8}$$

and then look up λ_0 in a table of $R_0(\lambda)$ vs. λ. The normalized product functions of Equation (8) for each filter, $[T(\lambda)H_1(\lambda)]$ and $[T(\lambda)H_1(\lambda)R_0(\lambda)]$, are shown in Figures 3-4 through 3-9, plotted as functions of λ. Also included are the numerical values of the integration over λ.

After the geometric factors have been folded in, we obtain the final test results as shown in Table 3-1. The "ratio" column gives the sensitivity of the SEC Vidicon photocathode as compared to the assumed "standard" S-20 tube.

Table 3-1
CATHODE RADIANT SENSITIVITY

λ_0, Å	HAO Tube ma/watt	Typical ma/watt	Ratio
4007	61.6	65.1	0.95
5267	56.7	46.7	1.22
6195	33.4	30.5	1.09

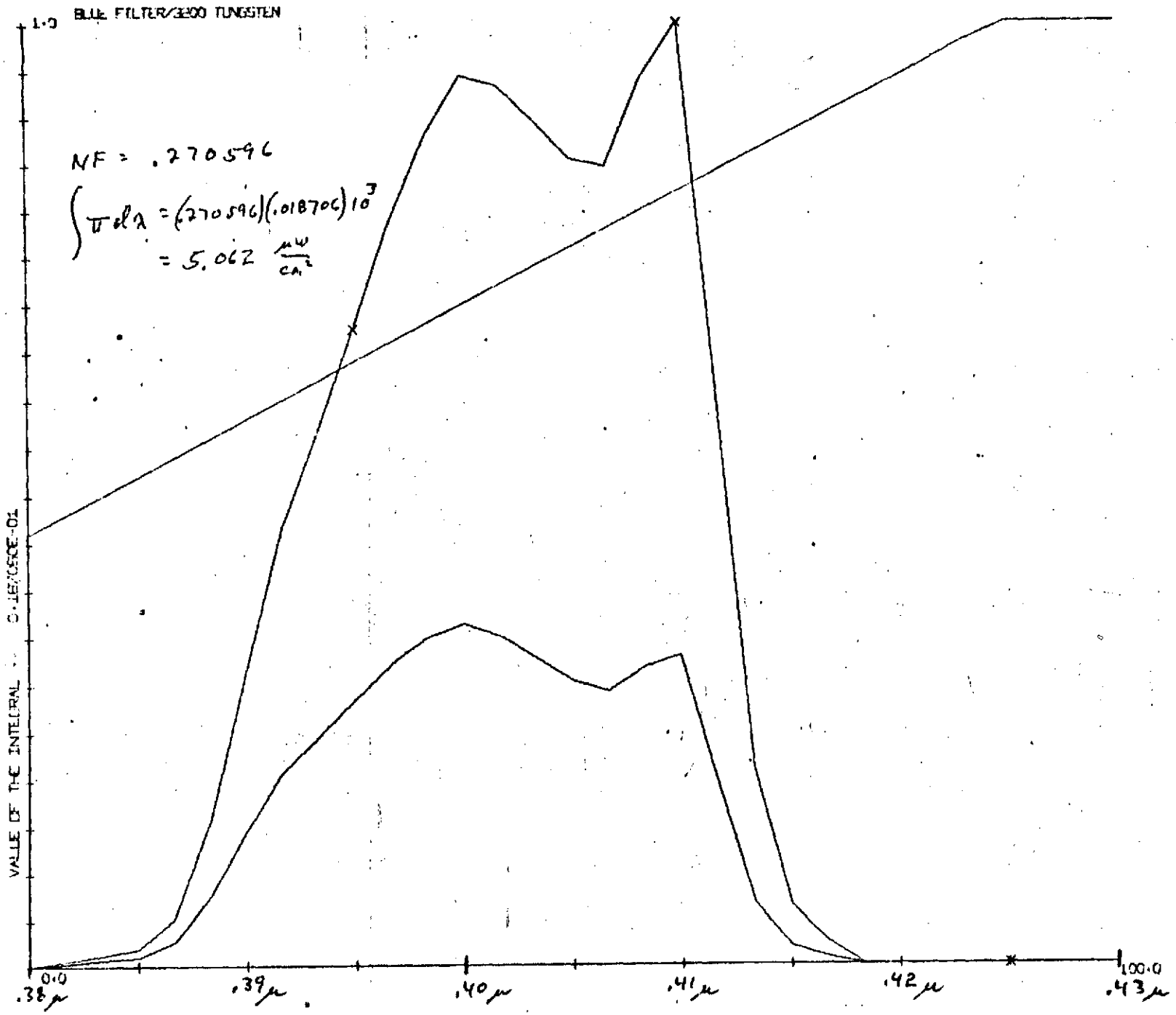

Fig. 3-4 Product Function $T(\lambda)H_1(\lambda)$ - Blue Filter

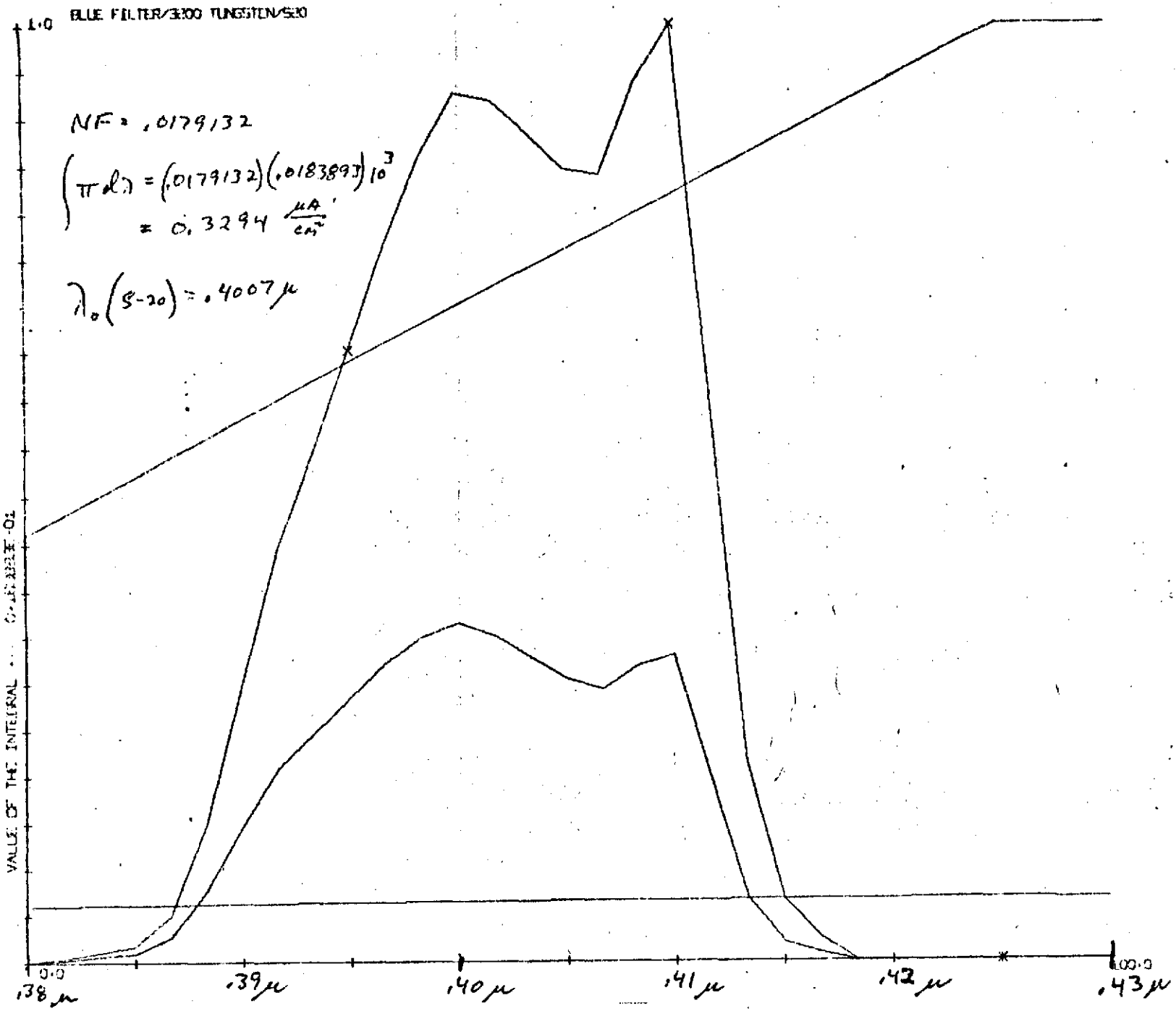

Fig. 3-5 Product Function $T(\lambda)H_1(\lambda)R_0(\lambda)$ - Blue Filter

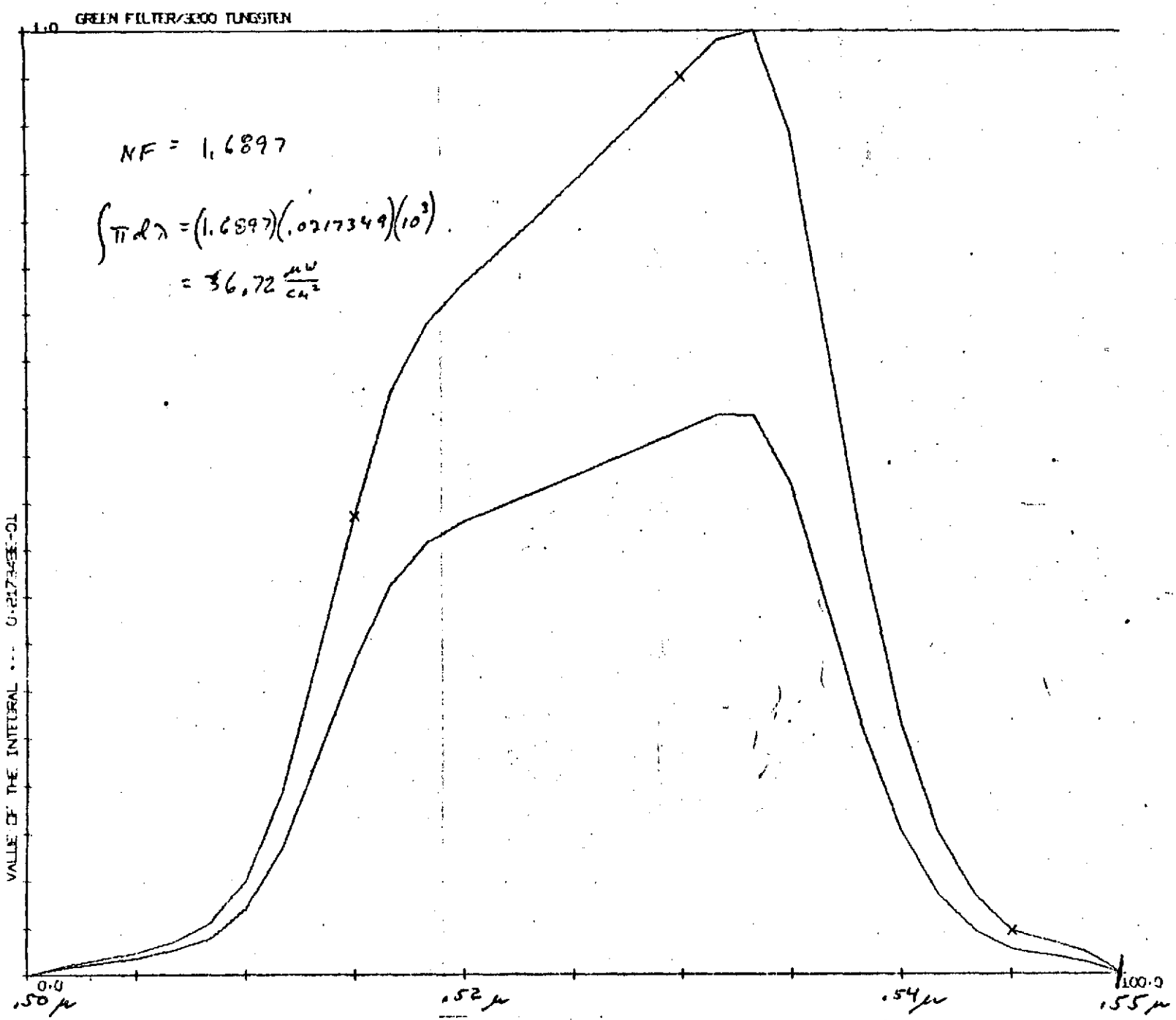

Fig. 3-6 Product Function $T(\lambda)H_1(\lambda)$ - Green Filter

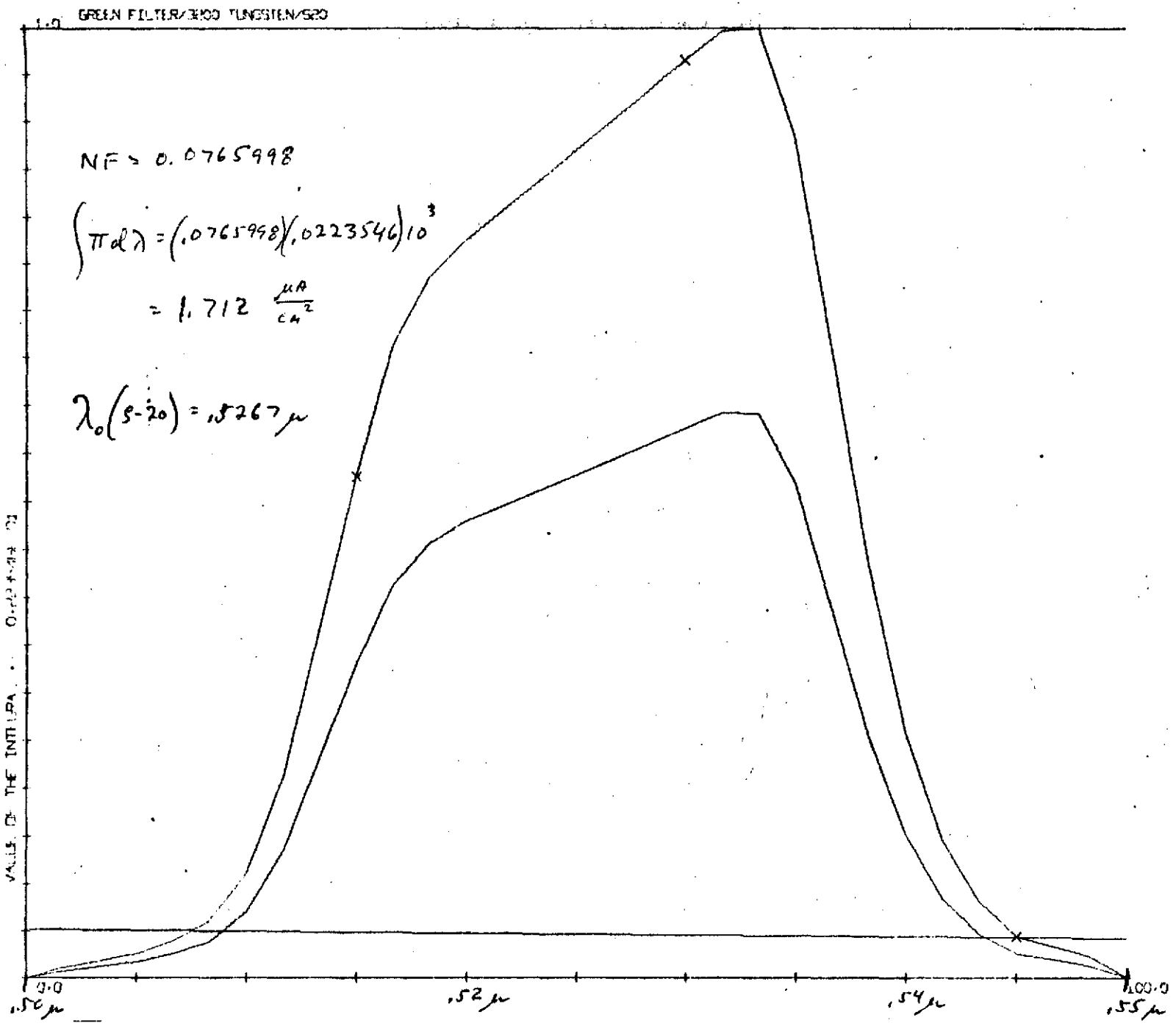

Fig. 3-7 Product Function $T(\lambda)H_1(\lambda)R_0(\lambda)$ - Green Filter

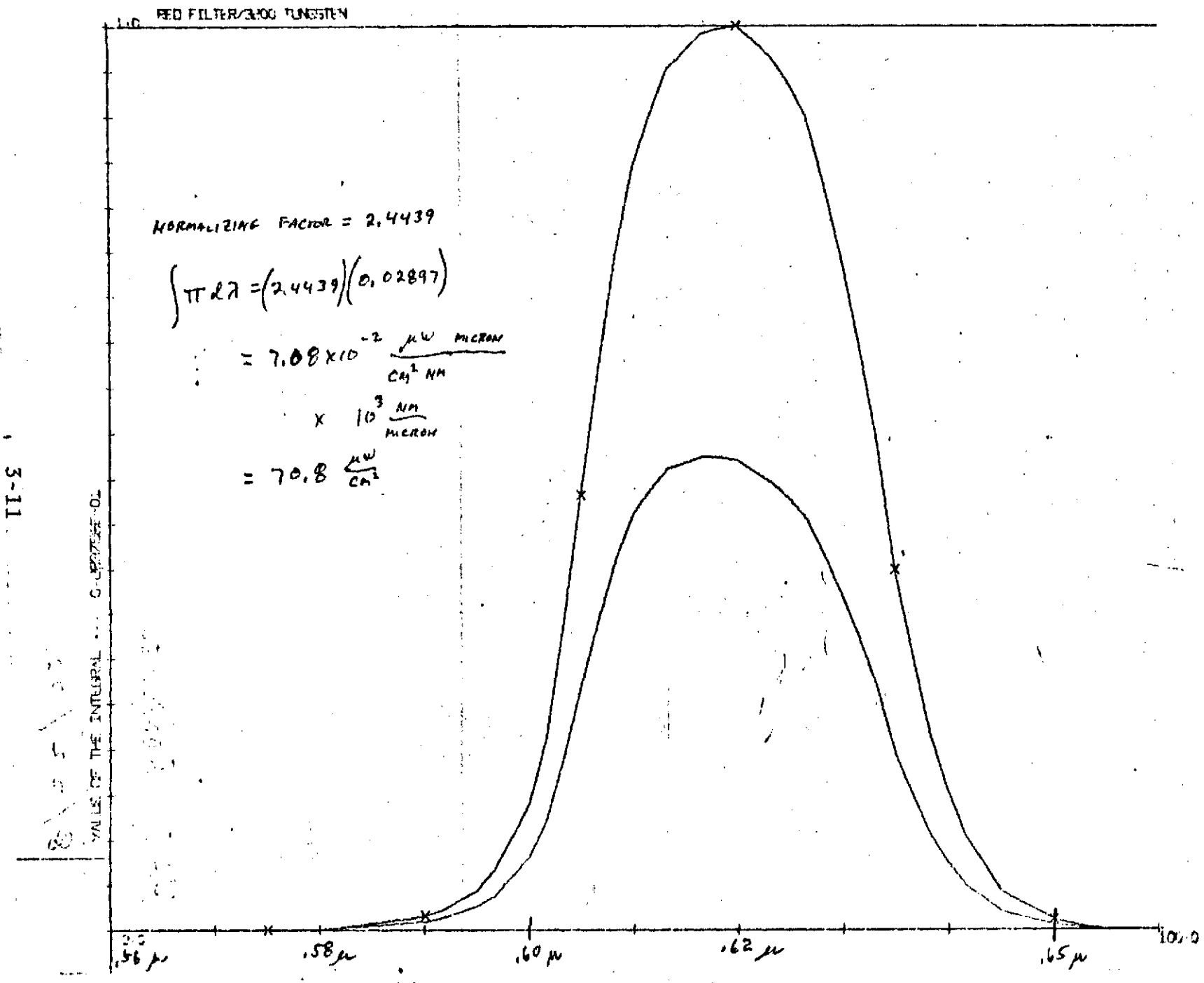

Fig. 3-8 Product Function $T(\lambda)H_1(\lambda)$ - Red Filter

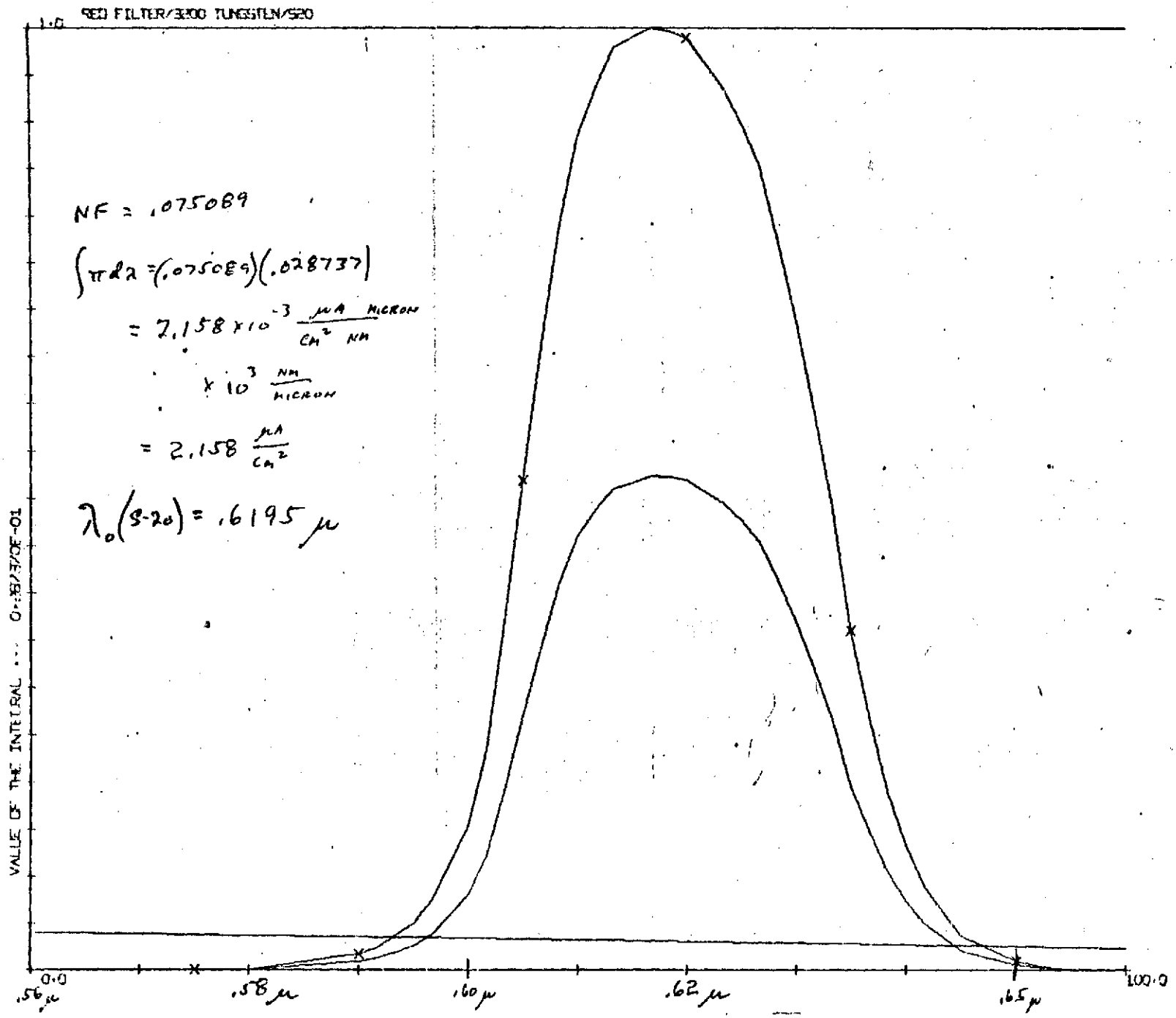

Fig. 3-9 Product Function $T(\lambda)H_1(\lambda)R_0(\lambda)$ - Red Filter

3.2 INPUT-OUTPUT

The input-output function of the SEC Vidicon camera system was determined in order to find the linear range of operation. Auxiliary calculation can then be used to show where normal tube operation would fall on this curve when used in conjuction with a flight-type coronagraph.

For the test, the input irradiance is varied while the output signal voltage from the complete camera head is monitored. There are two key requirements: one is that the input flux to the photocathode be known and variable, and the second is that it not change spectral characteristics as the level is changed. These requirements are difficult to meet simultaneously at the low light levels required. The test, therefore, was run in two stages. In the first, the electroluminescent panel in the microprojector was used as a source. It does not change color with intensity, but its absolute radiance was unknown. This source permitted plotting a curve of output current vs. irradiance, but without absolute scales.

The scales were obtained by the second-stage test, itself a process involving three steps:

1) A UDT Model 11A radiometer, which is linear over seven decades, was calibrated using the irradiance standard at a distance of 144.8 inches from the radiometer (Figure 3-10a). This gave input irradiances (integrated over λ) of about $10^{-8} w/cm^2$, varying with the filter used. The UDT reading was divided by the input radiance to give a calibration factor at each wavelength.

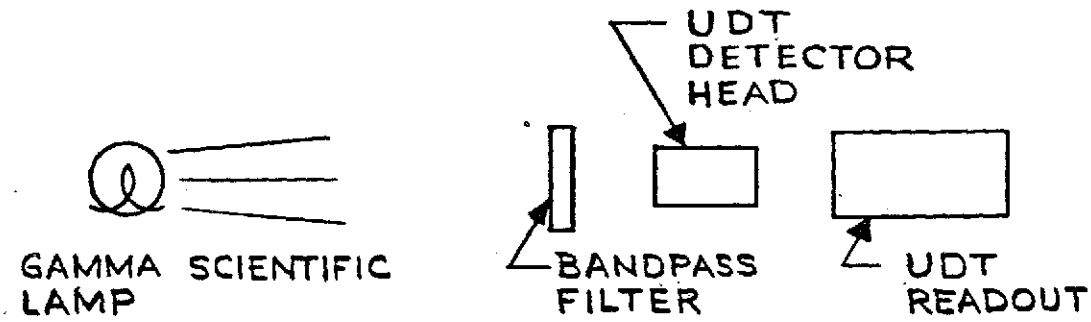

Fig. 3-10a Input-Output Configuration (Step 1)

2) The same lamp was used to irradiate a 7-inch diameter disc, coated with a diffusing white paint (Figure 3-10b). The UDT detector was used to measure the irradiance produced 189.8 inches from the diffuser.

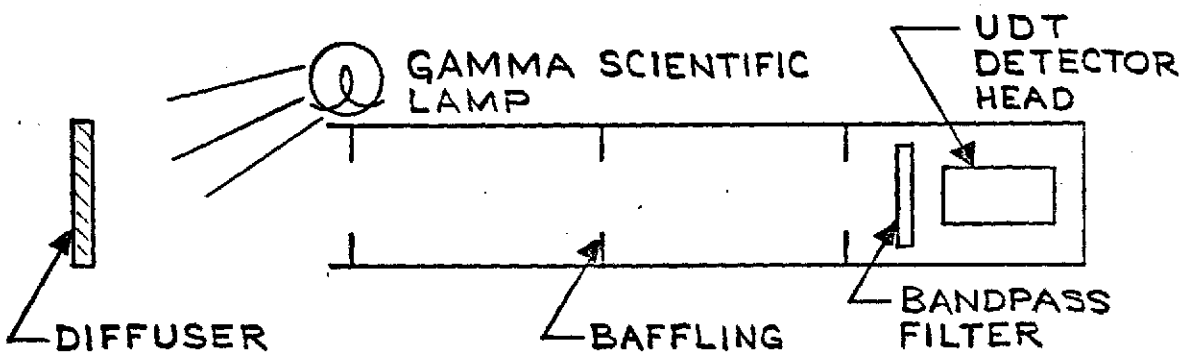

Fig. 3-10b Input-Output Configuration (Step 2)

3) The last step is substantially as Step 2, except the SEC Vidicon tube replaced the UDT detector, and an added stop reduced the irradiance to produce a near full-scale signal output from the camera head (Figure 3-10c).

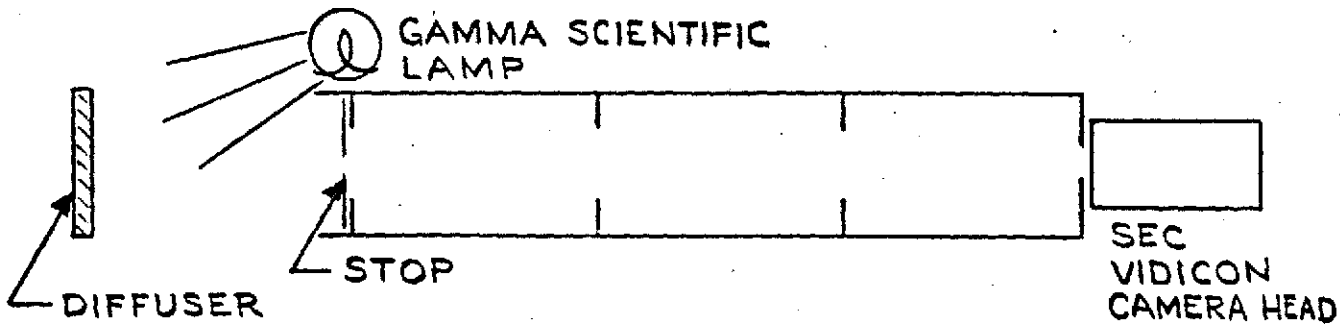

Fig. 3-10c Input-Output Configuration (Step 3)

The resulting input-output characteristics for each filter are shown in Figure 3-11.

In order to relate the signals expected from the solar corona to the operating region of the vidicon shown in Figure 3-11, we use the expression

$$H_I(\lambda) = \pi B(\lambda)\eta\overline{T}/4f^2 \qquad (9)$$

where

$H_I(\lambda)$ = Spectral irradiance of image (watt/cm^2-μ)

$B(\lambda)$ = Spectral radiance of corona (watt/cm^2-ster-μ)

η = Optical efficiency of coronagraph (exclusive of filters)

f = f-number of image space.

For fairly narrow bandwidths we can again use the idea of effective wavelength. We define $\Delta\lambda$ to be the effective bandwidth[5] of the filter used, and obtain for the total irradiance H_T

$$H_T = H_I(\lambda)\Delta\lambda \qquad (10)$$

or, substituting from Equation (9),

$$H_T = \pi B(\lambda)\eta\Delta\lambda/4f^2 \quad (\text{watt/cm}^2) \; . \qquad (11)$$

Interpolating from Allen, Astrophysical Quantities, Section 84, and summing the K and F coronas at a distance of six solar radii,

---

[5] $T'\Delta\lambda = \int T(\lambda)d\lambda$ where $T' = 1.0$.

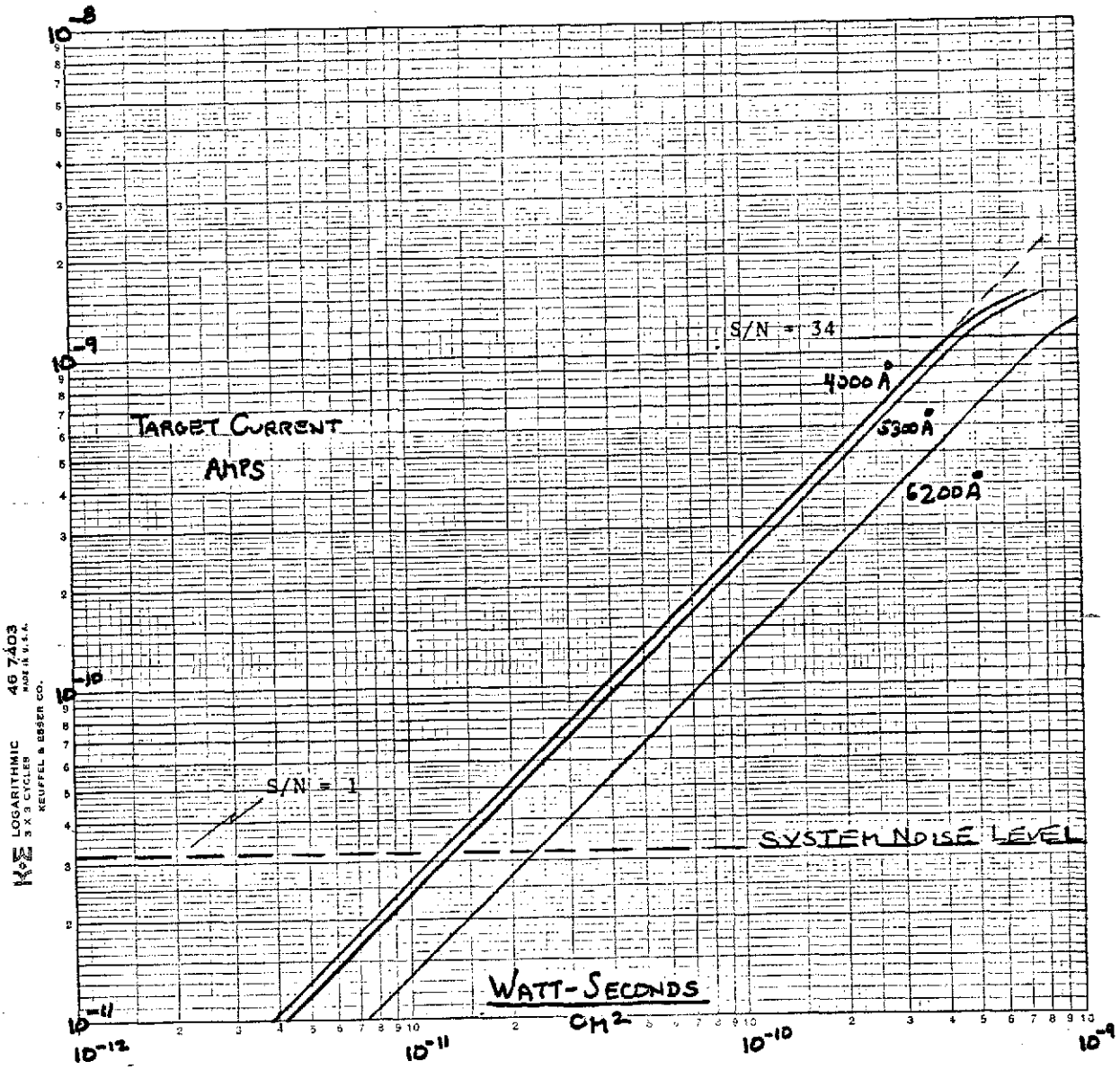

Fig. 3-11 Input-Output Characteristics of SEC Vidicon

we obtain a radiance of about 4.5×10^{-10} that of the mean solar disc. If we assume an f/33 coronagraph and $\eta = 0.42$, then Table 3-2 summarizes the values of the H_T for each filter and the other quantities entering into Equation (11).

Table 3-2
SPECTRAL IRRADIANCE IN FOCAL PLANE OF CORONAGRAPH FOR r = 6R

λ_0 (μ)	Solar Spectral Radiance$_1$* (watt/cm^2-sr-μ)	$\Delta\lambda$ (μ)	H_T (watt/cm^2)
0.4007	2.38×10^3	0.67×10^{-2}	2.2×10^{-12}
0.5267	2.95×10^3	1.36×10^{-2}	5.5×10^{-12}
0.6195	2.64×10^3	1.51×10^{-2}	5.4×10^{-12}

* Allen, C. W., Astrophysical Quantities, Athlone Press, 1963.

The filters used in these tests were not optimized for system use, but were merely narrow-band filters which were readily available. For system use, the filters must reject line radiation at 4861 Å (H_β), 5876 Å (He_I), and 6563 Å (H_α), but pass as much radiation as possible between these lines. In the violet and green, at least, suitable filters are commercially available with effective bandpasses of about 0.028 μ and 0.035 μ, respectively.

Table 3-3 provides exposure times for S/N of 1 and 34 (the upper limit of the linear region of Figure 3-11). Times are listed for each of the test filters, the alternate violet and green filters, and approximate times for unfiltered operation.

Table 3-3
EXPOSURE TIME vs. S/N for f/33 CORONAGRAPH

λ,μ	Time for S/N = 1, sec	Time for S/N = 34, sec
0.4007	5.4	191
0.5267	2.4	84
0.6195	3.8	156
violet	1.2	43
green	1.1	36
Unfiltered	0.11	4

3.3 TARGET GAIN

The target gain is an important parameter of the camera tube, indicating the average number of electrons stored on the target for each photoelectron received from the cathode. It can be computed from the results of the cathode radiant sensitivity and system radiant sensitivity measurements discussed in Sections 3.1 and 3.2. To do this, it must be remembered that the target both amplifies and stores (integrates) the charge pattern it receives from the photocathode during the exposure time, $(\Delta t)_E$. The output signal I_0, however, is a function of the rate at which the charge that is stored on the target is scanned by the readout beam, as well as reflecting any spatial variations in the charge density. Thus, the scan, or readout time, $(\Delta t)_R$, must be known.

Ignoring the spatial variation for simplicity, the photoelectron density accumulated during an exposure is given by:

$$\int_{t_1}^{t_2}\int_{\lambda_1}^{\lambda_2} H_{FP}(\lambda,t)R(\lambda)\,d\lambda\,dt \qquad (12)$$

If the faceplate irradiance H_{FP} is constant during an exposure, then we have for the "input" photoelectron density:

$$q(\Delta t)_E \int_{\lambda_1}^{\lambda_2} H_{FP}(\lambda)R(\lambda)d\lambda \quad \left(\frac{\text{photo-electrons}}{\text{cm}^2}\right) . \tag{13}$$

On the other hand, the "output" electron density is

$$q/A_s \int_0^{(\Delta t)_R} i_0(t)dt, \tag{14}$$

where A_s is the scanned area.

Assuming uniform illumination (spatially) and unity magnification, this becomes simply

$$\frac{qI_0(\Delta t)_R}{A_s} = \frac{qI_0(\Delta t)_R}{A_{PC}} \quad \left(\frac{\text{electrons}}{\text{cm}^2}\right) \tag{15}$$

where A_{PC} is the illuminated area on the photocathode. The target gain is merely the ratio of the output charge density to the input exposure

$$G_T = \frac{I_0(\Delta t)_R}{A_{PC}(\Delta t)_E \int_{\lambda_1}^{\lambda_2} H_{FP}(\lambda)R(\lambda)d\lambda} . \tag{16}$$

The results of this computation for the three applicable wavelength integrals are listed in Table 3-4 along with the actual photocurrents and output currents. The close grouping of the gain numbers from the three independent spectral measurements indicates the good consistency of our radiometric measurements. These values of gain are typical of SEC targets for the voltages used during these tests.

TABLE 3-4
TARGET GAIN RESULTS

SEC OUTPUT CURRENT AT $4(10^{-10})$ WATT-SEC / CM^2 ON PHOTOCATHODE 4 SEC READOUT TIME		PHOTOCATHODE CURRENT AT 10^{-10} WATT/CM^2 - LIMITING APERTURE AREA = 2.85 CM^2	TARGET GAIN I_O/I_K
	I_O	I_K	
4000 Å	(1.06×10^{-9} AMP)	1.757×10^{-11} AMP	60.4
5300 Å	0.97×10^{-9} AMP	1.615×10^{-11} AMP	60
6200 Å	0.55×10^{-9} AMP	9.51×10^{-12} AMP	57.8

3.4 MODULATION TRANSFER FUNCTION (MTF)

A preliminary measurement of the MTF characteristic was made by scanning the resolution bars in the Baum pattern and also the USAF test pattern. A photograph of a typical line-trace across the Baum chart is shown in Figure 3-12. It is important to note that these data do not represent the ultimate resolution capability of the tube since it was taken with the field mesh (and wall electrode) operating at potentials far below what is considered necessary for maximum resolution. The reason for operating the readout section at such low voltage stems from the fact that we are working with a Class III or "set-up" tube which has a defect which could lead to tube damage if operated at normal potentials.

A plot of the square-wave MTF as measured from these line-trace waveforms is given in Figure 3-13. Also shown is a response curve measured by Westinghouse on the same tube at 30 frames/second. The upper curve shows a response typical of that reported by Lowrance and Zucchino of Princeton with the same type of tube operated at optimum potentials.

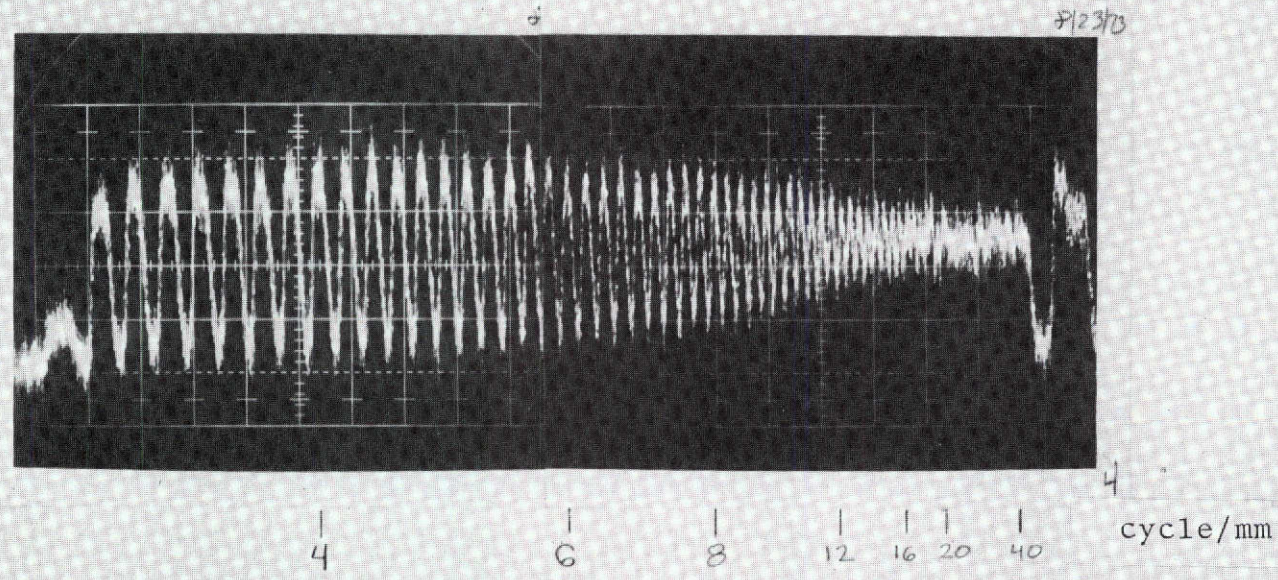

Fig. 3-12 Analog Output from Scan Across Baum Target

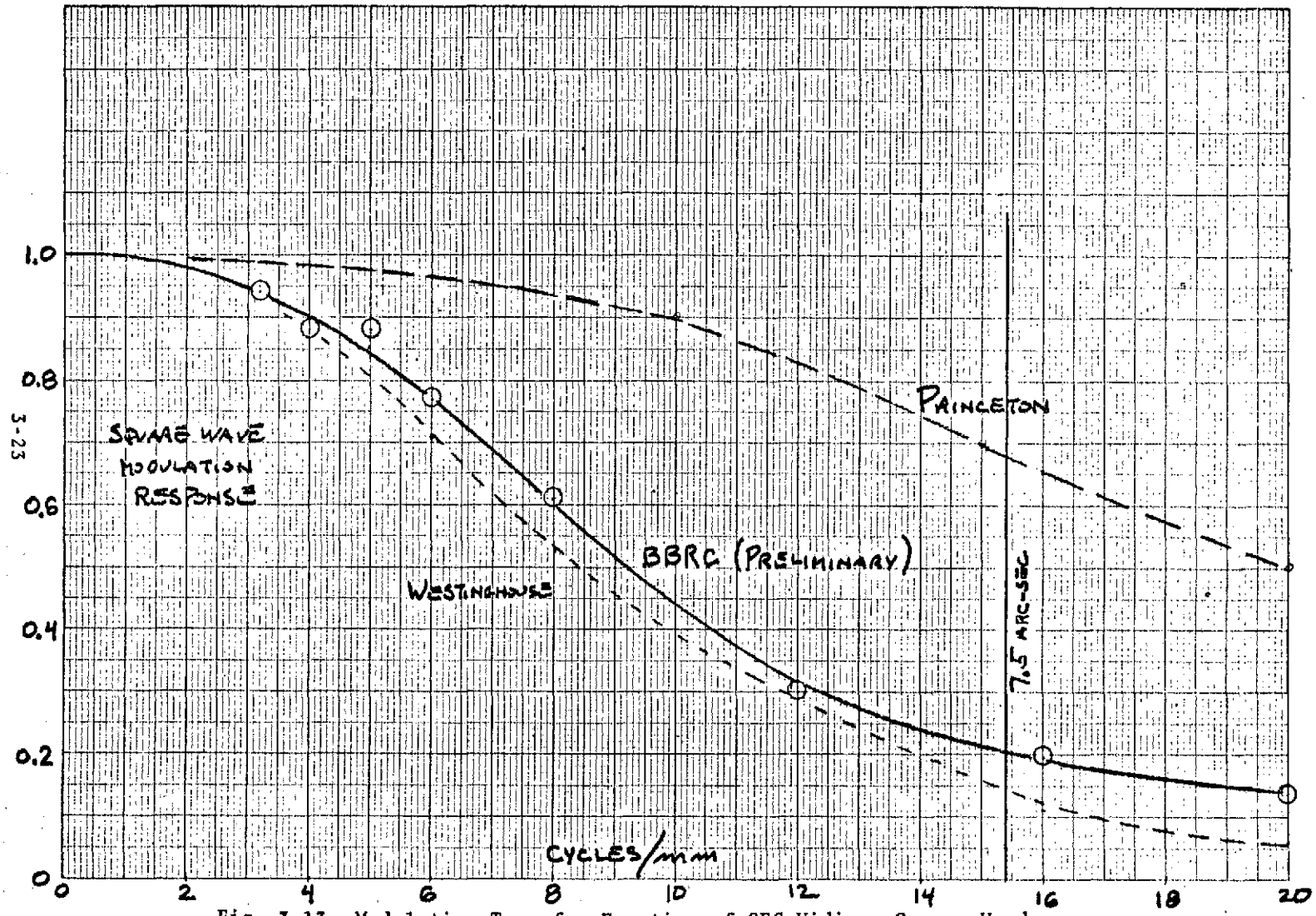

Fig. 3-13 Modulation Transfer Function of SEC Vidicon Camera Head

3.5 SIGNAL-TO-NOISE RATIO (S/N)

Using a four second readout time, the maximum usable output signal from our particular tube is set by its target saturation characteristic at about 1.5×10^{-9} Amp, as illustrated by the measured transfer characteristic plotted in Figure 3-11. On the other hand, the minimum usable signal level is not determined by the sensor itself but by the system background noise level. The latter is established primarily by the target-signal preamplifier, but it also exhibits some spurious components of interference from the test console sweep circuits and power supplies.

Low level, slow-scan systems such as this are very sensitive to this kind of interference and the design of any flight instrument must be intimately concerned from the outset with proper grounding and shielding against all forms of EMI.

The present system noise level is equivalent to about 33×10^{-12} Amp RMS target current, as measured with a wide-band true-RMS voltmeter. Tangential noise measurement techniques[6], using oscilloscope traces of the output, are in agreement with this number. Scope photographs of line traces taken at signal levels in the lower part of the transfer characteristic are shown in Figure 3-14. (These traces are from the data used to plot the curves in Figure 3-11.) From top to bottom the waveforms shown represent S/N ratios of approximately 17, 4, 2.3 and 1. In the top picture, photon noise is beginning to exceed that from the preamplifier. In the lower three traces, amplifier noise alone dominates. Reduction of the preamplifier noise can substantially increase the range over which the performance is predominantly photon-noise limited.

---

[6] A technique for RMS noise measurement using an oscilloscope. The random noise signal is mixed with an adjustable-amplitude square-wave signal and the sweep rate is set to result in two parallel noise traces on the scope screen. The two traces are moved toward each other until the dark lane between them just disappears. The RMS noise value is then one-half the square-wave amplitude.

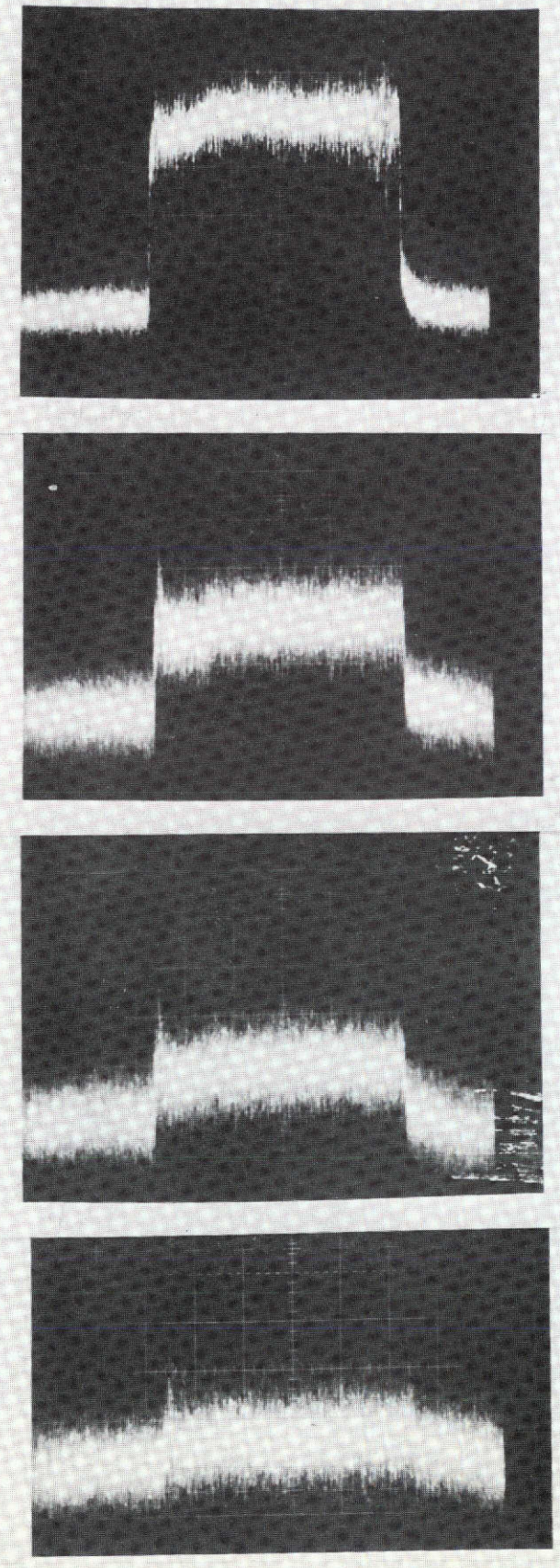

Fig. 3-14 Variation of Signal-to-Noise Ratios

3.6 AUXILIARY RESULTS

In addition to the five basic camera head tests, several auxiliary results were also obtained which are described in the following paragraphs. Included are results on cathode uniformity, various sources of noise encountered during the tests, and several miscellaneous results.

Cathode Mapping

Some indication of the photocathode uniformity was obtained by operating the camera tube image-section as a photodiode, as described in Section 3.1. The tube was mounted on an X-Y traverse fixture and the photocathode scanned manually with a small light spot about 0.51 mm in diameter. Two orthogonal scans were made approximately through the center of the faceplate and two additional horizontal scans were made 8 mm above and below the center line. The results are plotted in Figures 3-15a,b.

Noise Sources

It has already been discussed that any conductive or radiative source of interference can adversely affect system performance. This is especially true in slow scan operation. In the coronagraph we are working with, input signals fall in the range from 10^{-11} to 10^{-9} Amp over a frequency band from d.c. to 75 KHz. In order to take full advantage of the performance of the best state-of-the-art preamplifier, unwanted signals coupled in from extraneous sources must be kept below 10^{-12} Amp. (The only exception would be coherent noise sources which occur only during the horizontal or vertical blanking intervals.)

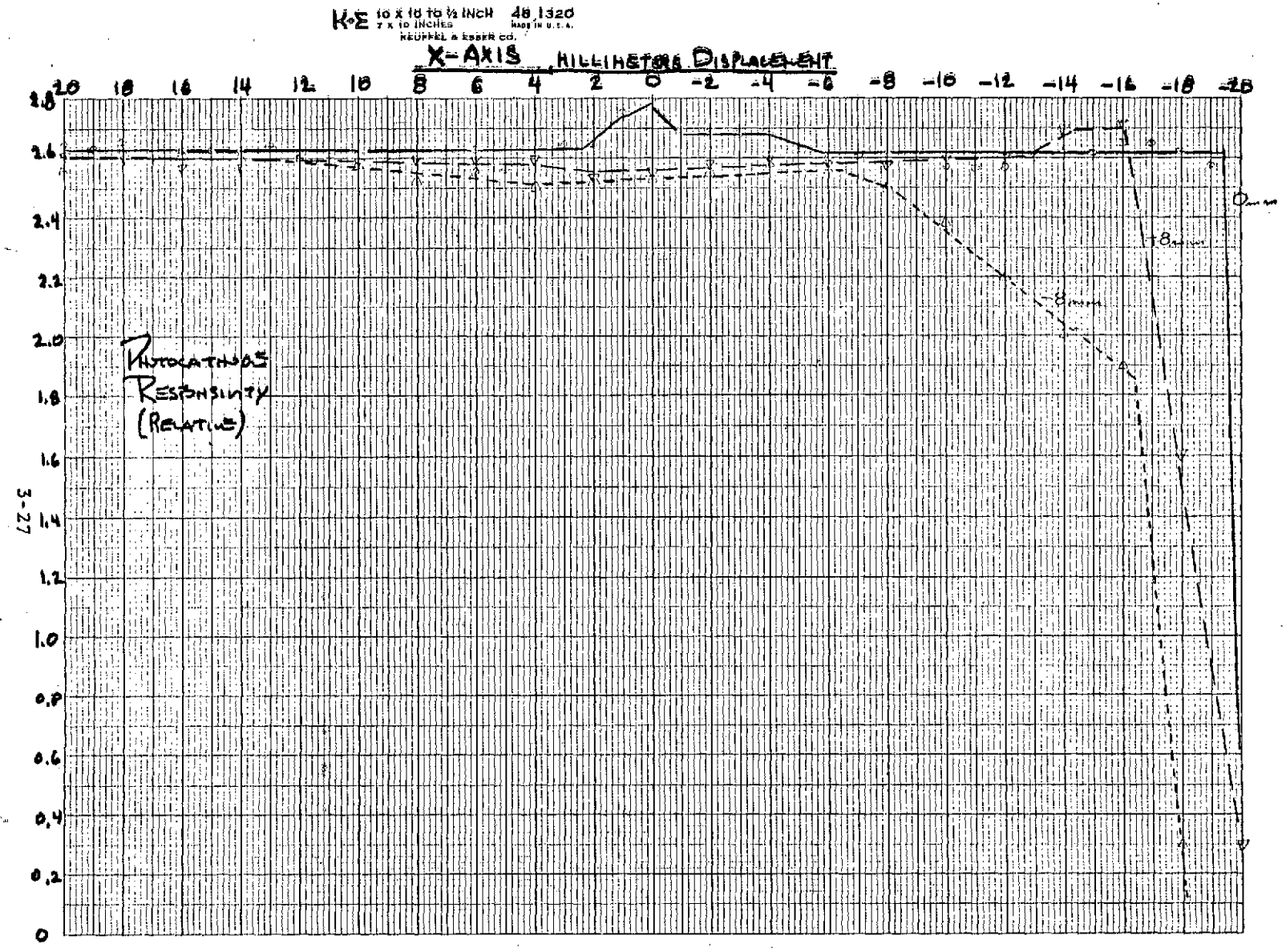

Fig. 3-15a Relative Photocathode Sensitivity (x-axis scans)

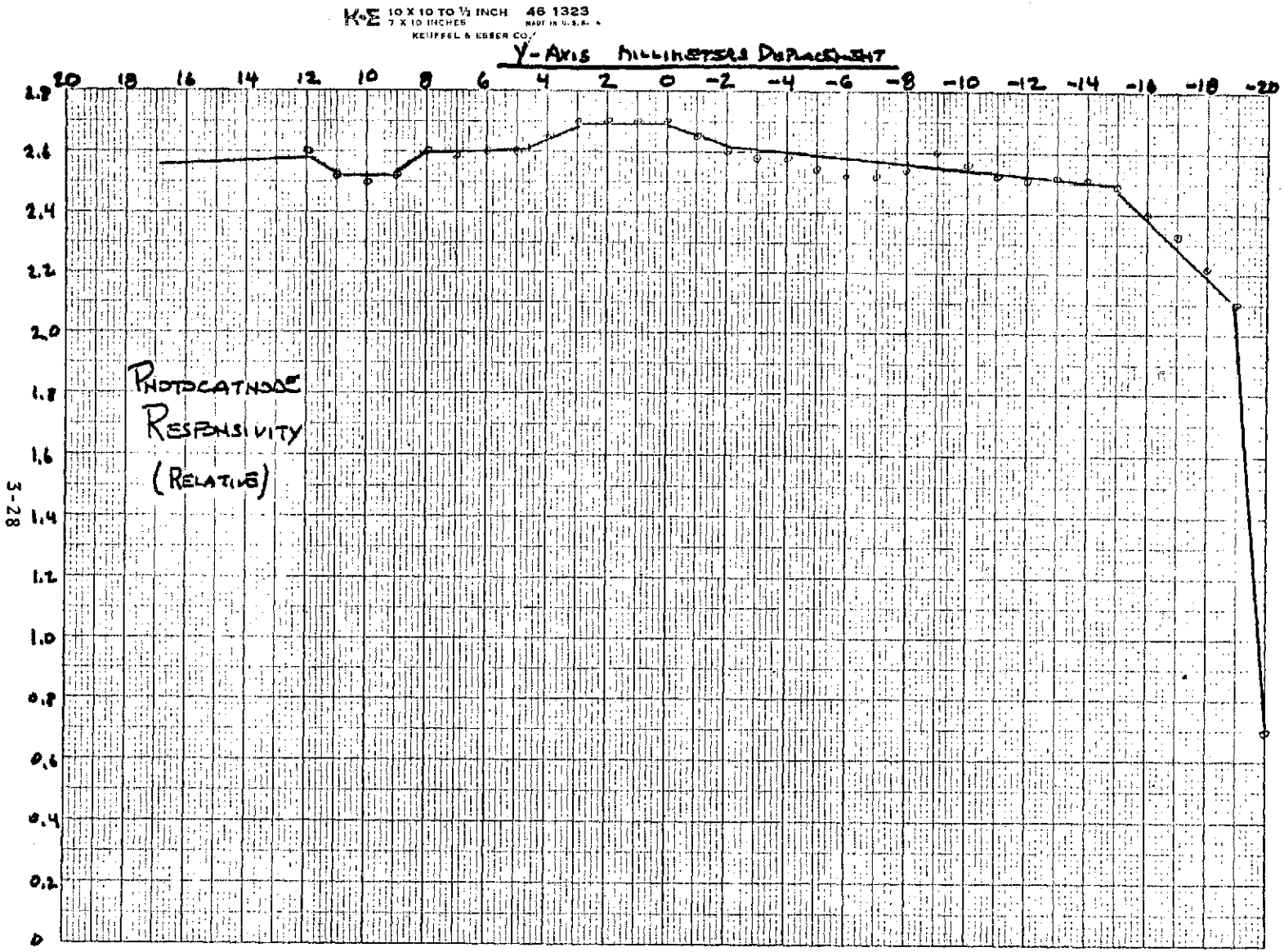

Fig. 3-15b Relative Photocathode Sensitivity (y-axis scan)

In addition to amplifier and pickup sources of noise, there are some significant ways in which considerable noise can be generated in the sensor itself, if it is not being operated properly. The two most obvious ways this can happen are described below. These sources can be distinguished from amplifier and pickup noise in that they only appear when the sensor is actually being scanned and then only in the illuminated or "highlight" areas of the target.

Line Bunching or Jitter

This is the effect of minute ripple components on the sweep signals. It can go undetected in ordinary 30 frame/second systems but can become quite serious in slow-scan operation. It is especially evident in applications such as the coronagraph where the line scan rate is in the neighborhood of 60 Hz or a low-order harmonic of this power line frequency. These power components effectively "beat" with the deflection signals, resulting in variation in line spacing across the tube. With a high resolution system this can cause variations of residual charge between lines, resulting in a clearly visible flutter or chatter in the line scan output while traversing a uniformly illuminated area on the faceplate. In the dark areas, of course, this effect is not visible. A ripple component of 0.1% in the vertical sweep would be serious in a high resolution (1000 line) system such as the coronagraph. Thus, it appears that the specification of ripple content must be well below 0.01% of the peak-to-peak sweep amplitude, as determined by overall image quality requirements.

Waterfall Effect

This source of noise also appears only in highlight portions of the scannned area. It is apparently caused when a well-focused readout beam lands fairly "hard" on the target but not perfectly

perpendicular to it. Thus, it is very dependent on how well the beam is aligned to assure that landing is normal to the target surface. It is also helped by operation with a high field-mesh potential which "stiffens" the beam and helps to maintain proper landing out at the corners of the scanned area. While the cause may be rather subtle, the effect is definitely not, as evidenced in Figure 3-16 showing two different degrees of its manifestation. (In this figure the black level is up and the white level down.) The effect is certainly striking and emphasizes the importance of proper set-up and operation of this sensor.

Miscellaneous Results

During the course of this project, several miscellaneous results were obtained which are described as follows:

- Development of set-up, operating, and safety procedures for this meshless type of SEC camera tube.

- Successful operation in both continuous-scan mode and single frame readout-multiple erase cycle mode.

- Verification of irradiance level-exposure time reciprocity over a ten-to-one range of exposure times.

- Identification and correction of problem areas in test set. (provides inputs to corresponding flight hardware).

- Development of a set of radiometric standards and absolute calibration procedures.

- Incorporation of microprojector as part of the test set-up. It is used to accurately project optically focused test targets on the sensor image plane and can be easily varied over a wide range of irradiance levels.

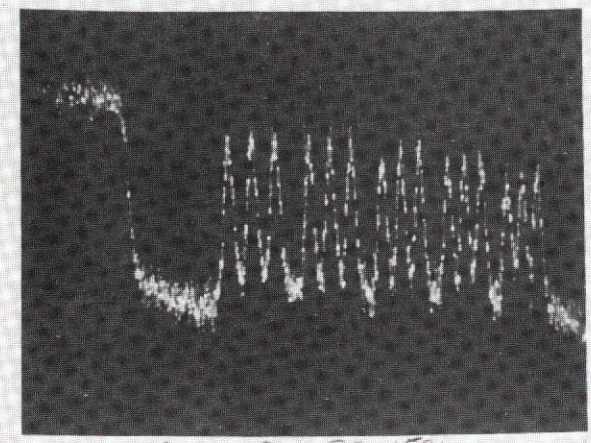

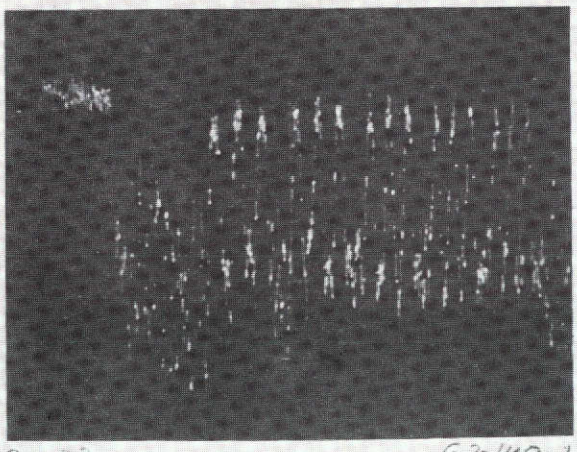

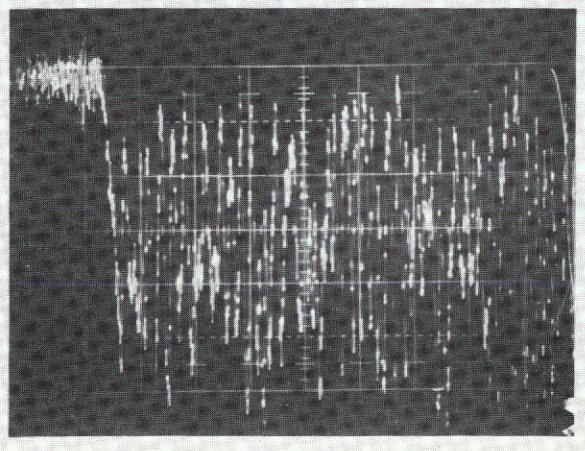

Fig. 3-16 "Waterfall" Noise

- Detailed knowledge of the regulation and ripple requirements of the current and voltage supplies needed for proper operation of the tube.

- Knowledge of the ways noise can contaminate the performance of low-level, slow-scan imaging systems.

Section 4
CONCLUSIONS

Based upon the present measurements of the SEC vidicon camera-head performance, several conclusions can be reached concerning its application in a rapid response coronagraph. These conclusions are summarized as follows:

- The meshless SEC vidicon tube will satisfy the sensor requirements for the RRC, but the camera head electronic system requires additional improvements.

- Overall system noise must be reduced. The specific areas requiring improvement involve the preamplifier noise and the noise associated with powerline pick-up in the sweep circuits.

- In addition to improving the dynamic range at the low end of operation by reducing system noise, the upper limit of operation (near saturation) can also be extended. In this sense, the ultimate flight vidicon should have the highest possible target capacitance in order to increase the maximum useable integration time.

- The time resolution of the RRC involves a trade-off between spectral bandpass, signal-to-noise ratio, radial distance of the observation from the center of the sun, and the presence of a polarization sensing element.

- Full performance in terms of spatial resolution (MTF) and signal-to-noise is not obtainable at the low mesh potentials which were required for the present measurements involving a Class III tube.

- It is important to obtain measurements of the camera head performance for such parameters as geometric distortion, variation in sensitivity over the image format, highlight spreading, temperature effects, and so forth.